PCCP

PAPER

View Article Online
View Journal | View Issue

Cite this: *Phys. Chem. Chem. Phys.*, 2025, **27**, 18454

Injection rate control on the growth direction in chemical gardens

Yujin Kubodera,[a] Muneyuki Matsuo [ab] and Satoshi Nakata *[a]

Received 21st May 2025,
Accepted 28th July 2025

DOI: 10.1039/d5cp01908g

rsc.li/pccp

The spontaneous organization of inorganic structures holds potential for applications in biomimetic material design. In this study, tubular precipitation structures were produced by injecting an aqueous solution of copper chloride into an aqueous solution of sodium silicate within an upright Hele–Shaw cell. The direction of tube growth, either upward or lateral, depended on the injection rate. The mechanism for selecting the growth direction and its bifurcation was examined in relation to factors such as the injection rate, water penetration, and the density differences between the two reactive solutions. This investigation contributes to the understanding of controlled inorganic spontaneous organization. It paves the way for diverse and autonomous growth in response to their environmental conditions, akin to plant growth or vascular formation in living organisms.

Introduction

Chemical gardens are notable for their ability to spontaneously organize characteristic structures under non-equilibrium conditions.[1–27] Nonlinear phenomena such as excitation,[3] oscillation,[4,5] and pattern formation[6–12] are observed in these systems. The resulting precipitates have shown potential for various applications, including quantum dots,[13] cell culture media,[14] microfluidic tubes,[15–18] and memristor devices.[19] In conventional chemical gardens, inorganic tubes form when metal salt particles are placed at the bottom of an aqueous silicate solution.[1,2] Using vertically oriented Hele–Shaw cells enables visualization of elemental distributions,[20] allows for the formation of microfluidic labyrinths,[18] characteristic filament shapes,[21] and both upward and downward growths.[22] A brief mechanism of the tube growth can be described in three steps.[23–25]

(Step 1) A semipermeable membrane forms around the metal salt particles through the precipitation of metal ions and silicate or hydroxide ions.[21]

(Step 2) Osmotic pressure builds up between the internal metal salt solution and the external aqueous silicate phases, leading to partial rupture of the membrane.

(Step 3) A new tube grows from the ruptured site.

Recent chemical garden experiments have been conducted by injecting the internal solution into the external solution.[12–17,26–29] This method of injecting the internal solution rather than placing the particles at the bottom of the chamber allows for quantitative control over the tube shape and growth as it eliminates the particle dissolution process, thus simplifying the system.[11–17,26–29] When the solution is injected from below, the tube grows from the injection point. In most studies, the growth direction is determined by the density difference between the injected and external solutions, *i.e.*, the tube grows upward[12–17,26,27] when the injected solution is less dense than the external solution. In contrast, the tube grows laterally[28] when the injected solution is denser than the external solution. Horváth *et al.* reported that upward tube growth can also occur when a denser metal salt solution is injected, due to water penetration into the tube.[29] However, the precise control of this water penetration has not yet been achieved.

In this study, we developed an experimental setup that enables control over the growth direction—either upward or lateral—by injecting a denser metal salt solution into an external solution, with the injection rate used to modulate water penetration. An aqueous solution of copper chloride ($CuCl_2$) was injected from the bottom of an upright Hele–Shaw cell, which consisted of two parallel glass plates with a narrow vertical gap filled with an aqueous solution of sodium silicate (Na_2SiO_3). Although the injected $CuCl_2$ solution was denser than the Na_2SiO_3 solution (external solution), the upward and lateral tube growth was observed, depending on the injection rate. We discuss the relationship between the direction of tube growth (upward or lateral) and water penetration. This study offers a strategy for designing novel inorganic tubes capable of diverse and autonomous growth in response to their environmental conditions.[30–33]

[a] *Graduate School of Integrated Sciences for Life, Hiroshima University, 1-3-1 Kagamiyama, Higashi-Hiroshima, Hiroshima 739-8526, Japan. E-mail: nakatas@hiroshima-u.ac.jp*
[b] *Graduate School of Arts and Sciences, The University of Tokyo, 3-8-1 Komaba, Meguro, Tokyo 153-8902, Japan*

Experimental

$CuCl_2{\cdot}2H_2O$ and Na_2SiO_3 were purchased from NACALAI TESQUE, Inc. (Kyoto, Japan). Water was purified using activated carbon (PF carbon cartridge, Organo Corporation, Tokyo, Japan), an ion-exchange resin (G-5D, Organo Corporation, Tokyo, Japan), and a Millipore Milli-Q filtering system (Merck Direct-Q 3UV, Germany; resistance: 18.2 MΩ cm). A Hele–Shaw cell (thickness: 1 or 2 mm, width: 64 mm, and height: 42 mm) was constructed using two slide glasses (thickness: 1.3 mm, width: 76 mm, and height: 52 mm; S9213, MICRO SLIDE GLASS, Matsunami Glass Ind., Osaka, Japan) and a silicone sheet (thickness: 1 and 2 mm; K-125, Togawa Rubber Co. Ltd, Osaka, Japan and 6-611-04, AS ONE Corp., Osaka, Japan, respectively) as a spacer. A needle (PN-27G-B, Musashi Engineering, Inc., Tokyo, Japan; inner diameter: 0.2 mm and length: 13 mm) was inserted at the center of the bottom of the cell (Fig. 1).

The tip of the needle penetrated 2 mm into the Hele–Shaw cell through a spacer. The other side of the needle was connected to a syringe pump (YSP-301, YMC Co., Ltd, Kyoto, Japan; minimum and maximum injection rates were 0.023 and 153.3 μL min^{-1}) *via* a silicone tube (LABORAN(R) Silicone Tube, AS ONE Co., Osaka, Japan; inner diameter: 3 mm and length: 200 mm). A 3 mL volume of 0.6 M Na_2SiO_3 aqueous solution was carefully poured into the upright Hele–Shaw cell until it was filled to the top. Subsequently, a $CuCl_2$ aqueous solution was injected into the cell through the needle. The tube growth was observed from the side using a digital video camera (HDR-CX430, SONY, Tokyo, Japan; minimum time resolution: 1/30 s) and analyzed using ImageJ software (National Institutes of Health, Bethesda, MD, USA). All experiments were conducted in an air-conditioned room at 298 ± 1 K. At least three trials were performed for each experimental condition to confirm the reproducibility of the observed phenomena.

Results

Direction of tube growth at different injection rates and $CuCl_2$ concentrations

First, we examined tube growth under varying injection rates, Q (μL min^{-1}), concentrations of the injected $CuCl_2$ aqueous solution, $[CuCl_2]_i$ (M), and densities, ρ_i (g mL^{-1}), of the $CuCl_2$ aqueous solution. Fig. 2a shows the time-variation snapshots recorded at t (s) under the conditions of Q = (a-i) 2.5, (a-ii) 5.0, and (a-iii) 20.0 μL min^{-1} at $[CuCl_2]_i$ = 1.3 M. Here, t is the elapsed time since the start of $CuCl_2$ injection. 1.3 M $CuCl_2$ aqueous solution was selected because its density ρ_i (= 1.14 g mL^{-1}) was higher than that of the external Na_2SiO_3 aqueous solution, ρ_{out} (= 1.05 ± 0.01 g mL^{-1}). At the initial stage of injection, a hemispherical dome (radius: 2–4 mm) was formed at the needle tip (see t = 100 s in Fig. 2a-i, and t = 50 s in Fig. 2a-ii and a-iii). At Q = 2.5 μL min^{-1}, a tube grew vertically from the needle to the top of the cell (Fig. 2a-i). At Q = 5.0 μL min^{-1}, the tube initially grew laterally along the base of the cell between t = 50 and 400 s, but then redirected and continued to grow vertically to the top of the cell (see t = 450 and 750 s in Fig. 2a-ii). At Q = 20.0 μL min^{-1}, the tube grew laterally across the cell to the other edge (see Fig. 2a-iii). Thus, three types of tube growth were observed based on the growth direction, *i.e.*, upward growth, upward growth following lateral one, and lateral growth.

Fig. 2b shows the phase diagram illustrating the observed growth types depending on $[CuCl_2]_i$, ρ_i, and Q in the range of $0.4 \leq [CuCl_2]_i \leq 2.0$ M, $1.05 \leq \rho_i, \leq 1.23$ g mL^{-1}, and $2.5 \leq Q \leq 20.0$ μL min^{-1} before the tip of the tube reached either the side edge or the top of the cell. The vertical solid line and gray region denote the mean value and standard deviation of ρ_{out}. No tube formation was observed at $Q < 2.5$ μL min^{-1}. Notably, the threshold values of Q separating upward and lateral growth modes decreased as $[CuCl_2]_i$ increased, as indicated by the dotted curve in Fig. 2b. The growth-type transition depended on the width of the Hele–Shaw cell, w_c. The range of Q in the upward growth for w_c = 2 mm ($2.5 \leq Q \leq 10.0$ μL min^{-1}, see Fig. S2b, SI) was larger than that for w_c = 1 mm ($2.5 \leq Q \leq 6.0$ μL min^{-1}, see Fig. S2a, SI). A dome-shaped structure with multiple upward tubes was observed when injecting 1.0 M

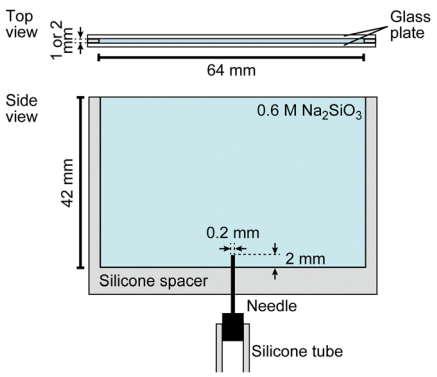

Fig. 1 Schematic illustration of the upright Hele–Shaw cell with a needle inserted at the center of the bottom to investigate the direction of the tube growth.

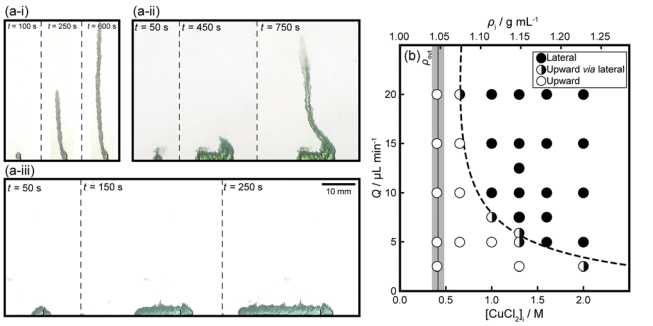

Fig. 2 (a) Time-variation snapshots of tube growth observed at Q = (a-i) 2.5, (a-ii) 5.0, and (a-iii) 20.0 μL min^{-1}, w_c = 1 mm (side view). (b) Phase diagram of upward (empty circles), upward growth *via* lateral one (half-filled circles), and lateral (filled circles) growth depending on $[CuCl_2]_i$, ρ_i, and Q at w_c = 1 mm. The upper axis refers to ρ_i. The vertical solid line and gray region denote the mean value and standard deviation of ρ_{out}. The dashed boundary curve in (b) was obtained using a support vector machine (SVM) with a polynomial kernel, highlighting the transition between upward and lateral growth. The movies of the tube growth in (a-i), (a-ii), and (a-iii) are provided in the SI as Movies S1, S2, and S3, respectively.

$CuSO_4$ aqueous solution whose density was similar to that of 1.3 M $CuCl_2$ at Q = 20.0 μL min^{-1}, w_c = 1 mm (Fig. S4, SI).

Relationships between the degree of water penetration, the density in the tube, and the injection rate

Next, the growth rate of the tube, V_r (μL min^{-1}), was measured as a function of Q and $[CuCl_2]_i$ to evaluate water penetration into the tube at w_c = 1 mm. V_r was calculated by least-squares fitting from the change in the tube area over time obtained by image analysis for 100 s before the tube reached the top or side edges of the cell. When calculating V_r, we confirmed that the width of all tubes was equal to the width of the Hele–Shaw cell, *i.e.*, 1 mm. $V_r = Q$ indicates that the tube volume is equal to the injection volume. Under the condition of $0.4 \leq [CuCl_2]_i \leq 1.0$ M at Q = 5.0 μL min^{-1} and $0.4 \leq [CuCl_2]_i \leq 2.0$ M at Q = 2.5 μL min^{-1}, V_r could not be calculated because the tube width was less than 1 mm. V_r was proportional to Q as the relationship $V_r = 1.3Q$ at $Q \geq 7.5$ μL min^{-1} (see the dotted line in Fig. 3a-i). In contrast, $5 \leq Q < 7.5$ μL min^{-1}, V_r was greater than $1.3Q$. V_r/Q was calculated to evaluate the degree of water penetration during tube formation. If the tube is formed without water penetration, V_r/Q should be 1. With an increasing Q, V_r/Q decreased at $5 \leq Q < 7.5$ μL min^{-1} and remained constant ($\sim$1.3) at $Q \geq 7.5$ μL min^{-1} (see Fig. 3a-ii). The density of the $CuCl_2$ aqueous solution in the tube, ρ_t, was estimated by the following two steps. First, the concentration of the $CuCl_2$ aqueous solution in the tube, $[CuCl_2]_t$, was estimated using $[CuCl_2]_i$, Q, and V_r, as indicated in eqn (1).

$$[CuCl_2]_t = [CuCl_2]_i \times Q/V_r \quad (1)$$

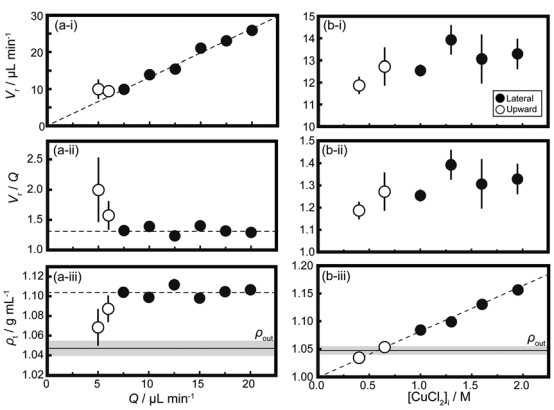

Fig. 3 (a) Relationships between (i) V_r, (ii) V_r/Q, and (iii) ρ_t depending on Q at $[CuCl_2]_i$ = 1.3 M, w_c = 1 mm. The dotted line in (a-i) denotes $V_r = 1.3Q$ obtained by the least-squares method performed on plots showing lateral growth. The dotted lines in (a-ii) and (a-iii) denote the average values of plots showing lateral growth, V_r/Q = 1.3 and ρ_t = 1.104 g mL^{-1}, respectively. (b) Relationship between (i) V_r, (ii) V_r/Q, and (iii) ρ_t depending on $[CuCl_2]_i$ at Q = 10.0 μL min^{-1}, w_c = 1 mm. The dotted line in (b-iii) denotes $\rho_t = 0.0826 \times [CuCl_2]_i + 0.997$ g mL^{-1}, obtained by the least-squares method performed on all plots. Empty and filled circles denote upward and lateral growth, respectively. The error bars denote the standard deviations obtained from three trials. The horizontal solid line and gray region in (iii) denote the mean value and standard deviation of ρ_{out}.

Here, we assume that only water molecules permeate the tube membrane.[24] Second, ρ_t was estimated by eqn (S1) using $[CuCl_2]_t$ (see Section S2 in the SI). As a result, ρ_t increased with increasing Q at $5 \leq Q < 7.5$ μL min^{-1} and remained constant ($\sim$1.104 g mL^{-1}) at $Q \geq 7.5$ μL min^{-1} (see Fig. 3a-iii). Both V_r and V_r/Q were almost independent of $[CuCl_2]_i$ (Fig. 3b-i and b-ii). On the other hand, ρ_t was proportional to $[CuCl_2]_i$ (see Fig. 3b-iii).

The above trend was also observed for w_c = 2 mm. The value of V_r/Q for w_c = 2 mm was higher than that of w_c = 1 mm at $7.5 \leq Q \leq 12.5$ μL min^{-1} (see Fig. 3a and Fig. S3, SI). The flow in the tube was laminar based on the calculation of the Reynolds number (see Section S5 in the SI for more details). The average membrane thickness, w_m, was observed at Q = 5.0 and 20.0 μL min^{-1}, $[CuCl_2]_i$ = 1.3 M, w_c = 1 mm in the range of 5–8 mm from the needle tip. As a result, $w_m = 0.42 \pm 0.08$ and 0.44 ± 0.03 mm at Q = 5.0 and 20.0 μL min^{-1}, respectively, *i.e.*, w_m was independent of Q.

Discussion

Based on the experimental results and related studies,[1,12,20–27] we discuss the characteristic tube growth in relation to the physicochemical parameters. While previous studies have demonstrated the contribution of osmotic permeation to tube formation,[29] our results reveal that the injection rate can modulate osmotic penetration, thereby controlling the growth direction of the tube by injecting a denser metal salt solution. In the following section, we discuss the dependence of the water penetration on the injection rate and its effect on determining the direction of tube growth.

Fig. 4 shows a schematic illustration of the mechanism underlying the upward and lateral growth. Initially, a semipermeable membrane is formed by the precipitation reaction with the Na_2SiO_3 aqueous solution,[23,24] as described in the following reactions (State I):

$$Cu^{2+} + 2OH^- \rightleftarrows Cu(OH)_2 \quad (2)$$

$$Cu^{2+} + SiO_3^{2-} \rightleftarrows CuSiO_3 \quad (3)$$

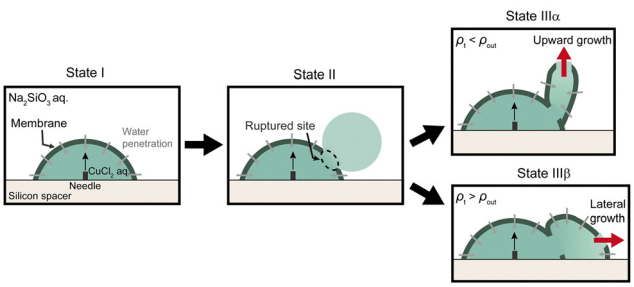

Fig. 4 Schematic illustration of upward and lateral growth. Water penetration is driven by the concentration difference between the inside and outside of the semipermeable membrane at State I. A part of the semipermeable membrane ruptures, and the $CuCl_2$ aqueous solution is then ejected to the outside at State II. When $\rho_t < \rho_{out}$, the tube tip is lifted up as shown in State IIIα. When $\rho_t > \rho_{out}$, the tube is laterally along the bottom of the cell, as shown in State IIIβ.

Next, water penetration from the external solution into the interior of the membrane occurs due to an ionic concentration gradient.[24] Both the injection of the $CuCl_2$ aqueous solution and this osmotic water influx cause swelling, which increases internal pressure. Eventually, the internal $CuCl_2$ aqueous solution is discharged *via* membrane rupture (State II). The expelled $CuCl_2$ aqueous solution then induces the formation of a new membrane around the ruptured site (State III).[12,23] Under conditions below the dotted line in Fig. 2b, the upward tube growth occurs even though the injected $CuCl_2$ aqueous solution is denser (ρ_i = 1.14 g mL^{-1} for $[CuCl_2]_i$ = 1.3 M) than the external Na_2SiO_3 aqueous solution (ρ_{out} = 1.05 ± 0.01 g mL^{-1}) (see Fig. 2a-i for Q = 2.5 μL min^{-1}). This upward growth is thought to occur because the density of the released internal solution—equal to ρ_t—is lower than ρ_{out} (State IIIα). This hypothesis is supported by the observation that ρ_t decreases with decreasing Q, reflecting enhanced water penetration at lower injection rates (see Fig. 3a). Water penetration occurs regardless of $[CuCl_2]_i$, and ρ_t falls below ρ_{out} at the low $[CuCl_2]_i$ values—for example, $[CuCl_2]_i \leq 0.6$ M at Q = 10.0 μL min^{-1} (see Fig. 3b). Near the threshold conditions represented by the dotted line in Fig. 2b, the tubes initially grew laterally before switching to an upward growth (see Fig. 2a-ii for Q = 5.0 μL min^{-1}). This behavior likely occurs because the released internal solution (ρ_t) is initially denser than ρ_{out}, leading to membrane formation along the bottom of the cell (State IIIβ).[28,29] However, over time, the state of the tube tip can transition from IIIβ to IIIα. As the tube elongates, the increased distance from the injection point may allow for greater water penetration, reducing ρ_t. Notably, even under conditions where $\rho_t > \rho_{out}$ (*e.g.*, $5 \leq Q \leq 6$ μL min^{-1} in Fig. 3a-iii), the upward growth can still occur. This may be attributed to the vertical orientation of the injection, which may promote the upward growth even when the internal solution is slightly denser than the external solution. Under the conditions above the dotted line in Fig. 2b, the tubes exhibited persistent lateral growth (see Fig. 2a-iii for Q = 20.0 μL min^{-1}). This suggests that the combination of Q and $[CuCl_2]_i$ under these conditions results in $\rho_t > \rho_{out}$ throughout the tube's propagation to the cell boundary. The relationship between V_r and Q is $V_r = 1.3Q$ in lateral growth at $[CuCl_2]_i$ = 1.3 M (see the filled circle in Fig. 3a-i and a-ii). This relationship suggests that the tube is swollen by 0.3Q due to osmotic water penetration. Several previous studies have reported a linear relationship between Q and V_r.[1,26,27,34] In contrast, our experimental results show that V_r/Q depends on Q. Both the range of Q in the upward growth and V_r/Q were larger with larger w_c (see Fig. 3a and Fig. S2, S3, SI) due to the increase in the contact area between the tube membrane and the external Na_2SiO_3 aqueous solution. The threshold value of V_r/Q in the tube growth for w_c = 1 (approximately 1.4, see Fig. 3a) was lower than for w_c = 2 (approximately 1.7, see Fig 3Sb, SI). As the increasing ratio of the membrane area of the tube for w_c = 1 mm in the same increase of the tube volume due to the water penetration is greater than that for w_c = 2 mm, the tube for w_c = 1 mm is easily broken rather than w_c = 2 mm. Physicochemical properties such as the viscosity of aqueous solution and the chemical composition of the semipermeable membrane for the lateral growth need to be clarified in future studies (see Section S4 in the SI).

Conclusions

The direction of tube growth was successfully controlled by adjusting the injection rate, which modulates the degree of water penetration. We employed a vertically oriented Hele–Shaw cell and a syringe pump to find three distinct types of chemical garden growth: upward, upward *via* lateral, and lateral growth. These growth-types were found to depend on the injection rate and the density of the injected solution. These results are discussed in relation to the degree of water penetration into the injected aqueous solution and the initial density difference between the internal $CuCl_2$ and external Na_2SiO_3 aqueous solutions. Our findings reveal that the degree of water penetration into the injected aqueous solution, modulated by the injection rate, directly affects the internal density of the growing tube. At the lower injection rates, greater water permeation into the $CuCl_2$ aqueous solution reduced its density, leading to upward tube growth, as the solution inside the tube became less dense than the external Na_2SiO_3 aqueous solution. In contrast, at higher injection rates, reduced water penetration preserved the higher density of $CuCl_2$ aqueous solution, resulting in lateral tube growth due to its continued density dominance over the Na_2SiO_3 aqueous solution. In most previous injection-based systems, the growth direction of the chemical gardens was statically controlled, as determined by the initial density difference between the solutions.[11,12,22–26] In contrast, our results demonstrated that the growth direction can be dynamically controlled, as it is governed by the injection rate. This study provides new insights into an inorganic system that mimics multidirectional growth found in nature, such as plant growth and angiogenesis.

Author contributions

S. N. supervised the study. Y. K., M. M., and S. N. planned the project and designed the experiments. Y. K. conducted the experiments. Y. K. analyzed data. Y. K. and S. N. wrote the original drafts. Y. K., M. M., and S. N. wrote, reviewed, and edited the manuscript.

Conflicts of interest

The authors declare no conflicts of interest.

Data availability

The data that support the findings of this study are provided in the SI.

Supplementary information available: Movies of tube growth, equation relating the concentration and density in aqueous $CuCl_2$ solution. See DOI: **https://doi.org/10.1039/d5cp01908g**

Acknowledgements

This study was supported by the Sasakawa Scientific Research Grant (2024-3024) from The Japan Science Society, the JST SPRING (JPMJSP2132) and JSPS KAKENHI (25KJ1877) to Y. K. Additional support was provided by JST ACT-X (JP24031207) and the MEXT Leading Initiative for Excellent Young Researchers (JPMXS0320230007) to M. M., as well as by JSPS KAKENHI No. 25K00918 and 24K22324, and the Cooperative Research Program of ''Network Joint Research Center for Materials and Devices'' (No. 20251018) to S. N.

References

1 L. M. Barge, S. S. S. Cardoso, J. H. E. Cartwright, G. J. T. Cooper, L. Cronin, A. de Wit, I. J. Doloboff, B. Escribano, R. E. Goldstein, F. Haudin, D. E. H. Jones, A. L. Mackay, J. Maselko, J. J. Pagano, J. Pantaleone, M. J. Russell, C. I. Sainz-Díaz, O. Steinbock, D. A. Stone and N. L. Thomas, *Chem. Rev.*, 2015, **115**, 8652–8703.

2 C. Pimentel, M. Zheng, J. H. E. Cartwright and C. I. Sainz-Díaz, *ChemSystemsChem*, 2023, **5**, e202300002.

3 Y. Ding, C. M. Gutiérrez-Ariza, C. I. Ignacio Sainz-Díaz, J. H. E. Cartwright and S. S. S. Cardoso, *Angew. Chem., Int. Ed.*, 2019, **131**, 6273–6279.

4 S. Thouvenel-Romans and O. Steinbock, *J. Am. Chem. Soc.*, 2003, **125**, 4338–4341.

5 J. Pantaleone, A. Toth, D. Horvath, L. RoseFigura, W. Morgan and J. Maselko, *Phys. Rev. E*, 2009, **79**, 056221.

6 F. Haudin, J. H. E. Cartwright, F. Brau and A. De Wit, *Proc. Natl. Acad. Sci. U. S. A.*, 2014, **111**, 17363–17367.

7 S. Hussein, J. Maselko and J. T. Pantaleone, *Langmuir*, 2016, **32**, 706–711.

8 S. Wagatsuma, T. Higashi, Y. Sumino and A. Achiwa, *Phys. Rev. E*, 2017, **95**, 052220.

9 P. Kumar, D. Sebők, Á. Kukovecz, D. Horváth and Á. Tóth, *Langmuir*, 2021, **37**, 12690–12696.

10 L. A. M. Rocha, L. Thorne, J. J. Wong, J. H. E. Cartwright and S. S. S. Cardoso, *Langmuir*, 2022, **38**, 6700–6710.

11 B. C. Batista, P. Cruz and O. Steinbock, *Langmuir*, 2014, **30**, 9123–9129.

12 B. C. Batista, A. Z. Morris and O. Steinbock, *Proc. Natl. Acad. Sci. U. S. A.*, 2023, **120**, e2305172120.

13 R. Makki, X. Ji, H. Mattoussi and O. Steinbock, *J. Am. Chem. Soc.*, 2014, **136**, 6463–6469.

14 B. Aslanbay Guler, Z. Demirel and E. Imamoglu, *Appl. Mater. Today*, 2023, **31**, 101743.

15 C. Ritchie, G. J. T. Cooper, Y. F. Song, C. Streb, H. Yin, A. D. C. Parenty, D. A. MacLaren and L. Cronin, *Nat. Chem.*, 2009, **1**, 47–52.

16 D. L. Long, R. Tsunashima and L. Cronin, *Angew. Chem., Int. Ed.*, 2010, **49**, 1736–1758.

17 G. J. T. Cooper, A. G. Boulay, P. J. Kitson, C. Ritchie, C. J. Richmond, J. Thiel, D. Gabb, R. Eadie, D.-L. Long and L. Cronin, *J. Am. Chem. Soc.*, 2011, **133**, 5947–5954.

18 S. Testón-Martínez, T. Huertas-Roldán, P. Knoll, L. M. Barge, C. I. Sainz-Díaz and J. H. E. Cartwright, *Phys. Chem. Chem. Phys.*, 2023, **25**, 30469–30476.

19 V. Patel, M. Patel, B. Busupalli and A. Solanki, *Langmuir*, 2024, **40**, 2311–2319.

20 W. Zhao and K. Sakurai, *ACS Omega*, 2017, **2**, 4363–4369.

21 L. A. M. Rocha, J. H. E. Cartwright and S. S. S. Cardoso, *Chaos*, 2022, **32**, 053107.

22 Y. Ding, C. M. Gutiérrez-Ariza, M. Zheng, A. Felgate, A. Lawes, C. I. Sainz-Díaz, J. H. E. Cartwright and S. S. S. Cardoso, *Phys. Chem. Chem. Phys.*, 2022, **24**, 17841–17851.

23 J. H. E. Cartwright, J. M. García-Ruiz, M. L. Novella and F. Otálora, *J. Colloid Interface Sci.*, 2002, **256**, 351–359.

24 F. Glaab, M. Kellermeier, W. Kunz, E. Morallon and J. M. García-Ruiz, *Angew. Chem., Int. Ed.*, 2012, **51**, 4317–4321.

25 J. H. E. Cartwright, B. Escribano, C. I. Sainz-Díaz and L. S. Stodieck, *Langmuir*, 2011, **27**, 3294–3300.

26 V. Kaminker, J. Maselko and J. Pantaleone, *J. Chem. Phys.*, 2014, **140**, 244901.

27 S. Thouvenel-Romans, W. van Saarloos and O. Steinbock, *Europhys. Lett.*, 2004, **67**, 42–48.

28 M. R. Bentley, B. C. Batista and O. Steinbock, *J. Phys. Chem. A*, 2016, **120**, 4294–4301.

29 E. Rauscher, G. Schuszter, B. Bohner, Á. Tóth and D. Horváth, *Phys. Chem. Chem. Phys.*, 2018, **20**, 5766–5770.

30 C. M. Rounds and M. Bezanilla, *Annu. Rev. Plant Biol.*, 2013, **64**, 243–265.

31 E. Del Dottore, A. Mondini, N. Rowe and B. Mazzolali, *Sci. Robot.*, 2024, **9**, eadi5908.

32 M. N. Nakatsu, R. C. Sainson, J. N. Aoto, K. L. Taylor, M. Aitkenhead, S. Pérez-del-Pulgar, P. M. Carpenter and C. C. W. Hughes, *Microvasc. Res.*, 2003, **66**, 102–112.

33 J. Pauty, R. Usuba, I. G. Cheng, L. Hespel, H. Takahashi, K. Kato, M. Kobayashi, H. Nakajima, E. Lee, F. Yger, F. Soncin and Y. T. Matsunaga, *EBioMedicine*, 2018, **27**, 225–236.

34 F. Haudin, J. H. E. Cartwright and A. De Wit, *J. Phys. Chem. C*, 2015, **119**(27), 15067–15076.

